Regular Article

PHYSICAL CHEMISTRY RESEARCH
Published by the
Iranian Chemical Society
www.physchemres.org
info@physchemres.org

Phys. Chem. Res., Vol. 13, No. 4, 783-796, December 2025
DOI: 10.22036/pcr.2025.535946.2708

Unveiling the Anti-Apoptotic Mechanism of Magnolialide as a Colorectal Cancer Inhibitor *via* Molecular Modeling, ADMET, and MMGBSA Analysis

H.D. Nguyen*

Faculty of Biology, Thai Nguyen University of Education, 24000, Thai Nguyen, Vietnam

(Received 20 July 2025, Accepted 12 October 2025)

Colorectal cancer poses a significant global health challenge, driving demand for innovative therapeutic strategies. Apoptosis, modulated by the key anti-apoptotic regulator Bcl-xL, serves as a critical target for the selective elimination of cancer cells and the overcoming of survival mechanisms. This study investigated the molecular action of magnolialide, a natural compound derived from *Magnolia grandiflora*, as a potential anti-colorectal cancer agent through its interaction with Bcl-xL (protein ID: 3QKD) using integrated computational methods. Molecular docking analysis revealed magnolialide's superior binding affinity (-7.65 kcal mol^{-1}) and optimal orientation at the 3QKD active site compared to 5FU (-3.58 kcal mol^{-1}). Dynamics simulations conducted over 100 ns confirmed sustained stability and consistent molecular interactions, reinforcing the reliability of the binding. ADMET profiling indicated favorable pharmacokinetics for magnolialide, characterized by high intestinal absorption, moderate distribution, and minimal metabolic interference, despite a lower maximum tolerated dose compared to 5FU. Toxicity assessments showed no mutagenic potential, further supporting its safety profile. DFT analysis revealed enhanced molecular reactivity for magnolialide (ΔE = 11.6296 eV) compared to 5FU (ΔE = 12.5089 eV), attributed to the smaller energy gap, indicating greater electron transition potential. These findings establish magnolialide as a promising candidate for colorectal cancer therapy *via* Bcl-xL-mediated apoptosis modulation.

Keywords: Anti-apoptosis, Colorectal cancer, Magnolialide, Molecular docking, Molecular dynamics

INTRODUCTION

Colorectal cancer ranks as the third leading contributor to global mortality, with over 1.9 million new diagnoses and 903,859 fatalities recorded in 2022, accounting for approximately one in ten cancer cases and deaths worldwide [1]. Multiple investigations demonstrate a global increase in colorectal cancer incidence and mortality, linked to elevated consumption of processed foods, red meat, and alcohol, alongside reduced physical activity and higher obesity prevalence [2,3]. While surgery is often the primary treatment for localized colorectal cancer, chemotherapy is also a key component of treatment, particularly for advanced stages [4]. However, while chemotherapy can extend life for many cancer patients, it can also impact quality of life due to these side effects. Therefore, the continuous search for safer and more effective anti-cancer drugs remains an urgent direction in the development of cancer-targeted medications [5].

Natural products, derived from living organisms, possess a wide array of chemical structures and biological activities, making them valuable sources for discovering new drug candidates. Their inherent structural diversity and biological relevance provide a foundation for developing novel therapies, particularly in addressing chronic and infectious diseases [6,7]. Magnolialide, a natural compound predominantly present in *Magnolia grandiflora*, exhibits cytotoxic activity against the human colorectal cancer cell line (Colo320DM) through apoptosis, a highly regulated process that eliminates unwanted or damaged cells in multicellular organisms [8]. However, the molecular mechanisms underlying the apoptosis activity of

*Corresponding author. E-mail: hungnd@tnue.edu.vn

magnolialide remain insufficiently clarified. Nowadays, network pharmacology emerges as a promising innovative method for investigating the multi-target mechanisms of natural compounds. This technique provides a systems-oriented framework to elucidate interactions of complex compound mixtures, such as those present in traditional medicinal systems, with multiple targets within the organism to achieve therapeutic outcomes. This approach proves particularly valuable for analyzing natural products, which frequently encompass diverse bioactive constituents capable of influencing various biological pathways [9-11].

Thus, this investigation sought to explore anti-colorectal cancer activity of magnolialide through integrated computational methods including molecular docking, dynamics simulations, and ADMET prediciton. Furthermore, MM-GBSA calculations of the chosen protein-ligand complexes were executed to obtain an understanding of protein stability and to identify potential structural alterations resulting from compound binding. Lastly, electronic and structural properties of the selected compounds were examined using the DFT method. These outcomes provide a basis for experimental validation and optimization of magnolialide as a potential therapy for colorectal cancer.

MATERIALS AND METHODS

Data Collection

The structure of magnolialide (molecular formula of $C_{15}H_{20}O_3$ and molecular weight of 248.1412 *m/z*, was collected from Pubchem database (https://pubchem.ncbi.nlm.nih.gov/). 5-Fluorouracil (5-FU), a chemotherapy drug approved to treat various cancers, possessing molecular formula of $C_4H_3FN_2O_2$ and molecular weight of 130.0179 *m/z*, was chosen as the comparative reference (Fig. 1).

Evaluation of the Biological Activity of Magnolialide

The evaluation of the biological activity of magnolialide against human colorectal cancer (Colo320DM cell line) has been carried out in the previous study [8].

Molecular Docking

Three-dimensional ligand structures were generated in .pdb format utilizing Biovia Discovery Studio Visualizer,

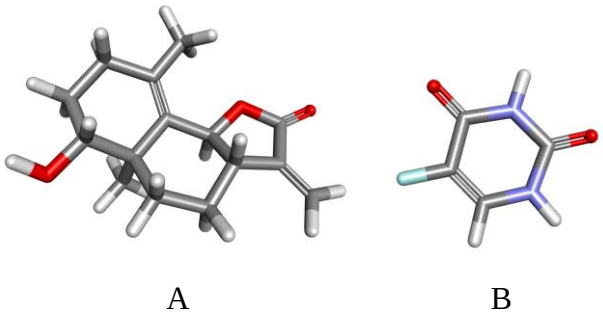

Fig. 1. 3D Structures of magnolialide (A) and 5FU (B).

with polar hydrogen atoms preserved, Gasteiger charges computed, and complete torsional flexibility assigned. The three-dimensional structure of Bcl-xL (B-cell lymphoma-extra large) (PDB ID: 3QKD) was obtained from the RCSB Protein Data Bank in .pdb format [12]. Structural integrity of the 3QKD protein was assessed by evaluating phi (φ) and psi (ψ) torsion angles through a Ramachandran plot generated using PROCHECK software [13]. Molecular docking of the protein and ligands was performed with AutoDock Tools, employing a grid box with dimensions x = 40, y = 40, z = 40, and a grid spacing of 0.375 Å. The docking site was defined at coordinates x = -10.980 Å, y = -19.200 Å, z = 8.807 Å within the 3QKD binding pocket. The Lamarckian genetic algorithm was applied to identify low-energy conformations for ligand-protein interactions.

Molecular Dynamics Simulation

Molecular dynamics simulations of the optimal docked conformation with the 3QKD protein were performed for 100 ns using GROMACS version 2024.4 with the CHARMM36 force field [14]. The protein structure was refined with Swiss-PdbViewer to correct missing atoms and residues [15]. Ligand topologies were generated through SwissParam [16]. The solvation system employed a triclinic simulation box tailored to the protein-ligand complex, utilizing the SPC water model and incorporating a 0.15 M sodium chloride concentration. Structural optimization and neutralization were achieved *via* 50,000 steps of energy minimization. System equilibration was conducted using a 200 ps NVT ensemble (constant particle number, volume, and temperature), followed by a 200 ps NPT ensemble (constant particle number, pressure, and temperature),

stabilizing at 300 K and 1.0 bar. Three independent simulations, each lasting 100 nanoseconds, were executed with a 2-femtosecond time step (0.002 ps), and trajectories were recorded every 10 ns. Analysis of simulation results was performed using Grace software to calculate parameters, including root mean square deviation (RMSD), root mean square fluctuation (RMSF) per residue, radius of gyration (Rg), number of hydrogen bonds (H-bonds), and solvent-accessible surface area (SASA). Conformational stability of the docked complexes was evaluated through structural alignment using UCSF Chimera version 1.1 [17].

Drug Likeness and ADMET Prediction

Drug likeness refers to the overall characteristics that make a compound suitable for drug development, including desirable physicochemical properties and favorable ADMET properties [18]. The pharmacokinetic and toxicological properties of selected iridoids were assessed using pkCSM, a web-based platform designed for predicting the drug-likeness of small molecules [19].

Molecular Mechanics Generalized Born Surface Area (MMGBSA) Analysis

The Molecular Mechanics Generalized Born Surface Area (MM/GBSA) method is a computational approach for estimating the binding free energy of a ligand with its target protein. Widely utilized in drug discovery and protein-ligand interaction studies, this method offers a balance between precision and computational efficiency [20]. It integrates molecular dynamics simulations with thermodynamic calculations to determine binding free energies. The MM/GBSA method, executed via gmx_MMPBSA with the charmm36-jul2022.ff force field, was employed to compute the binding free energy for the magnolialide-3QKD and 5FU-3QKD complexes. The Generalized Born model was used to calculate the electrostatic solvation energy in a continuum solvent environment, while the non-polar solvation energy was evaluated based on the solvent-accessible surface area. Binding free energy calculations were derived from 125 snapshots extracted at 80 ps intervals over an 80 ns molecular dynamics simulation period (from 20 to 100 ns). This approach provided an averaged binding energy, capturing the dynamic characteristics of protein-ligand interactions and facilitating the assessment of binding affinity and stability in a simulated environment.

Quantum Chemistry Computation Using the DFT Method

Density Functional Theory (DFT) experiences growing application within quantum computing frameworks to examine properties of lead compounds, enabling detailed analysis of electronic structures, molecular characteristics, and interactions. The integration of DFT with quantum computing provides an effective method for predicting and interpreting the behavior of lead-based materials across diverse applications [21]. Molecular structures of magnolialide and 5FU were subjected to energy minimization and full geometry optimization utilizing the ORCA 6.1.0 software package. Input files were prepared using Avogadro software and all energy calculations were executed within the ORCA environment, whereas output data underwent visualization and analysis *via* IboView v20211019 to improve comprehension of orbital distributions and molecular geometry [22-25]. DFT calculations occurred at the B3LYP level of theory, utilizing the 6-31G(d, p) basis set to accurately describe the electronic wave function of the molecules. Descriptors, including HOMO and LUMO energies, energy gap (ΔE), and additional reactivity parameters such as chemical potential (μ), electronegativity (χ), hardness (η), softness (σ), and electrophilicity index (ω), were calculated based on Koopmans' theorem [26,27].

RESULTS AND DISCUSSION

Protein Structure Preparation and Validation

A Ramachandran plot was generated utilizing PROCHECK software to assess the stereochemical integrity of the refined 3QKD protein structure, identified as Bcl-xL, a key regulator in the anti-apoptotic pathway linked to colorectal cancer cell viability. This plot delineates conformational regions based on the distribution of Φ and Ψ dihedral angles, which correspond to energetically favorable configurations of amino acid residues, derived from a dataset of high-resolution protein structures. The x-axis represents Φ angles, while the y-axis represents Ψ angles, collectively defining residue orientations. Analysis of the 3QKD structure revealed that 96.00% of non-glycine and non-proline

residues, totaling 241 residues, were located in the most favored regions (A, B, L), while 4.00% were positioned in the additionally allowed regions (a, b, l, p), corresponding to 10 residues. No residues were detected in the generously allowed regions (~a, ~b, ~l, ~p) or disallowed regions, each with zero residues, based on a total of 251 non-glycine and non-proline residues, representing 100.00% of this subset. The complete 3QKD structure comprises 282 residues, including 7 terminal residues (excluding glycine and proline), 20 glycine residues (depicted as triangles), and 4 proline residues (Fig. 2).

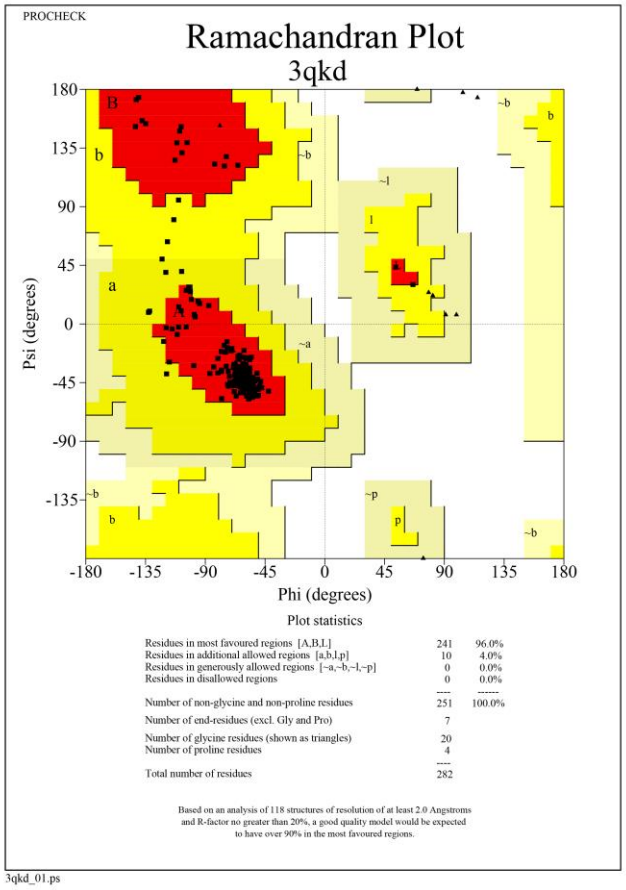

Fig. 2. Ramachandran plot of energy-minimized predicted structures of 3QKD.

This residue distribution aligns with standards established from the analysis of 118 protein structures with resolutions of 2.0 Å or better and R-factors not exceeding 20%, where a high-quality model is expected to have over 90% of residues in the most favored regions. The 3QKD structure satisfies this criterion, with 96.00% of residues in the most favored regions and no residues in disallowed regions (0.0%), confirming its conformational integrity. This structural stability supports its suitability for molecular docking and dynamics simulations, enhancing the precision of evaluating interactions between magnolialide and the Bcl-xL binding site. Consequently, this facilitates the assessment of magnolialide's potential to modulate the anti-apoptotic pathway and its efficacy as a therapeutic candidate for colorectal cancer treatment.

Docking Analysis

Molecular docking serves as an essential method in structure-based drug design, facilitating the prediction of binding interactions between small molecules and macromolecular targets. This approach determines the preferred binding conformation and estimates the associated binding free energy, which is vital for elucidating molecular interactions and informing drug development [28]. The present study analyzed the binding affinity and interactions of the 3QKD protein with magnolialide, using 5FU as a reference. Structural visualization of the 3QKD protein identified key active site residues, including Ala93, Glu96, Arg100, Tyr101, Phe105, Ser110, Gln111, Leu112, His113, Val126, Glu129, Leu130, Gly134, Asn136, Gly138, Arg139, Val141, Ala142, Phe191, and Tyr195 (Fig. 3A). Prior to docking simulations, the docking protocol for the 3QKD protein was validated through a redocking procedure involving the co-crystallized ligand, with results presented in Fig. 3B. The protocol's accuracy was confirmed by a root mean square deviation (RMSD) value of 1.6115 Å, derived from the superposition of the native and docked ligand conformations, indicating reliable docking performance. An RMSD value below 2 Å is generally accepted as a benchmark for successful docking poses in molecular docking studies [29].

The interactions of the magnolialide and 5FU with the binding pockets of the 3QKD protein are presented in Table 1. The specific amino acid residues involved in these interactions, along with their precise locations within the ligand-binding site, were identified. Molecular docking analysis revealed the occurrence of hydrogen bonds, van der

Table 1. Interactions of Docked Ligands with the 3QKD Protein

N°	Docked ligands	Binding energy (kcal mol^{-1})	Hydrogen bond interaction	Van der Waals interaction	Hydrophobic interaction
1	Magnolialide	-7.65	Val126	Phe97, Phe125, Glu129, Ser145	Ala104, Leu108, Val126, Leu130, Ala142, Phe146
2	5FU	-3.58	Phe105, Ala142, Ser145	Phe97, Glu98, Val126, Leu130, Phe143, Phe146, Ala149	Leu198, ALa142

Waals forces, and hydrophobic contacts between the protein and ligands, with each molecular interaction involving the 3QKD amino acid residues illustrated in Fig. 4.

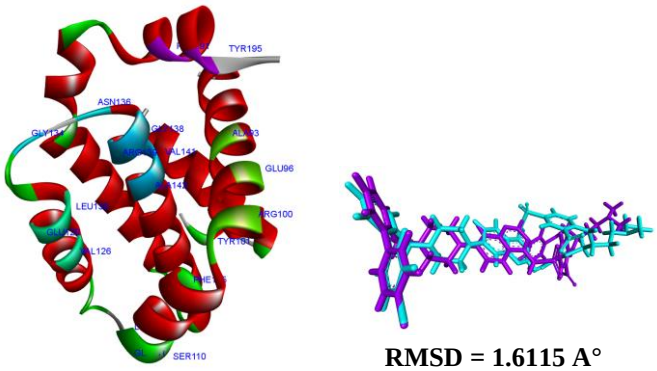

Fig. 3. Active sites within the 3QKD protein (A) and superimposition of the docked and native ligands for validation of the molecular docking protocol (violet = native, cyan = docked) (B).

Magnolialide demonstrated interactions with the 3QKD protein, forming a hydrogen bond with the amino acid Val126, four van der Waals interactions with residues Phe97, Phe125, Glu129, and Ser145, and six hydrophobic interactions with residues Ala104, Leu108, Val126, Leu130, Ala142, and Phe146. Of these, the residues Phe105, Val126, Glu129, Leu130, and Ala142 are situated within the active sites of the 3QKD protein (Fig. 4A). The binding free energy of magnolialide with the 3QKD protein was calculated to be -7.65 kcal mol^{-1}.

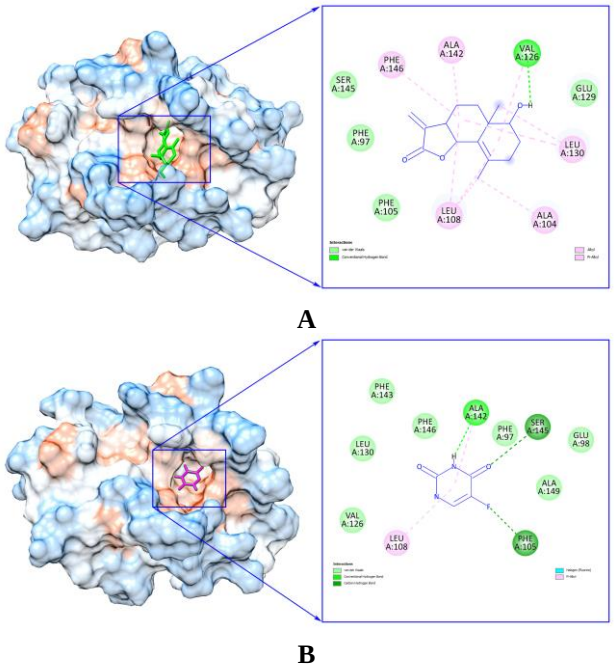

Fig. 4. Molecular docking and two-dimensional interaction schematics for magnolialide (A) and 5FU (B) in complex with the 3QKD protein.

5-Fluorouracil (5FU) formed interactions with the 3QKD protein, establishing three hydrogen bonds with residues Phe105, Ala142, and Ser145, seven van der Waals interactions with residues Phe97, Glu98, Val126, Leu130, Phe143, Phe146, and Ala149, and two hydrophobic interactions with residues Leu198 and Ala142. Of these, four residues, including Phe105, Val126, Leu130, and Ala142, are located within the active sites of the 3QKD protein. The binding free energy of 5FU with the 3QKD protein was determined to be -3.58 kcal mol^{-1} (Fig. 4B).

Molecular docking simulations of magnolialide and 5FU with the 3QKD protein revealed a variety of interaction types, including hydrogen bonds, van der Waals forces, and hydrophobic interactions, which collectively contribute to the stability of the ligand-protein complexes [30,31]. While hydrogen bonds exhibit greater strength and directional specificity, hydrophobic interactions provide significant stabilization, particularly at extensive protein-ligand interfaces. Van der Waals forces play a critical role in stabilizing ligand-protein complexes by facilitating precise spatial alignment, thereby enhancing binding affinity in conjunction with hydrogen bonds and hydrophobic interactions [32]. These noncovalent interactions are essential for achieving optimal docking configurations. A more negative binding free energy typically indicates a more stable and favorable binding event, reflecting stronger ligand retention within the receptor [33]. The docking results demonstrate that magnolialide, with a binding free energy of -7.65 kcal mol^{-1} and a total of 11 interactions (5 involving active site residues Phe105, Val126, Glu129, Leu130, and Ala142), exhibits superior binding affinity to the 3QKD protein compared to 5FU, which has a binding free energy of -3.58 kcal mol^{-1} and 12 interactions (4 involving active site residues Phe105, Val126, Leu130, and Ala142). The active site residues Val126, Leu130, and Ala142, where magnolialide forms robust interactions, are critical for modulating the anti-apoptotic activity of Bcl-xL, as they are located within the BH3-binding pocket of the 3QKD structure. These interactions likely interfere with the binding of pro-apoptotic proteins, such as BAX and BAK, which are essential steps in the apoptosis pathway, thereby enhancing the suppression of apoptosis resistance in colorectal cancer cells. The conservation of these active sites across Bcl-xL homologs, as observed in structural analyses, underscores their significance for translational research. Consequently, magnolialide emerges as a promising candidate for further molecular dynamics simulations, with 5FU serving as a reference compound to evaluate the stability and dynamic behavior of the ligand-protein complex within the Bcl-xL binding pocket, particularly at these key active sites.

Molecular Dynamics Simulation

Molecular dynamics simulations, performed using GROMACS, were utilized to investigate the binding characteristics of ligand-protein complexes. In this analysis, molecular dynamics simulations were conducted on the magnolialide-3QKD and 5FU-3QKD complexes to evaluate parameters including root mean square deviation (RMSD), root mean square fluctuation (RMSF), radius of gyration (Rg), hydrogen bonds (H-bonds), and solvent-accessible surface area (SASA). The total energy was determined to be -223,910 kcal mol^{-1} for the magnolialide-3QKD complex and -224,667 kcal mol^{-1} for the 5FU-3QKD complex. The potential energy values were calculated as -279,094 kcal $mol^{-1}$for magnolialide-3QKD and -279,791 kcal mol^{-1} for 5FU-3QKD. The system achieved equilibrium at a temperature of 300 K.

The RMSD serves as a vital metric for evaluating structural congruence between molecular configurations, particularly in molecular dynamics simulations and comparative structural analyses. It measures the average displacement of corresponding atoms across superimposed structures, with reduced RMSD values signifying enhanced structural alignment and greater similarity [34]. The RMSD trajectories for the magnolialide-3QKD and 5FU-3QKD complexes, observed over a 100 ns simulation period, displayed distinct characteristics (Fig. 5A). The magnolialide-3QKD complex exhibited RMSD values ranging from 0.2 to 0.3 nm, with a mean of 0.25 nm, indicating a stable structural configuration and robust binding interaction with the 3QKD protein. In contrast, the 5FU-3QKD complex showed RMSD values varying between 0.2 and 0.25 nm, averaging 0.225 nm, suggesting a slightly lower structural fluctuation while preserving adequate stability. This difference suggests that the magnolialide-3QKD complex maintains a more uniform conformational stability compared to the 5FU-3QKD complex, potentially indicating a stronger binding affinity within the 3QKD active site. Therefore, the observed RMSD patterns support the inference that the magnolialide-3QKD complex preserves its initial structure more effectively than the 5FU-3QKD complex, as confirmed by the current dynamic evaluation.

Figure 5B illustrates the RMSF profiles for the magnolialide-3QKD and 5FU-3QKD complexes, assessed over a 100 ns simulation period, with flexibility evaluated across residues Ser4 to Asn197, covering the entire polypeptide chain of the 3QKD protein. This variability likely associates with the spatial arrangement of these

residues relative to essential active binding sites, including significant positions such as Val126, Leu130, and Ala142. Specifically, the magnolialide-3QKD complex shows a decrease in RMSF from 0.12 nm to 0.05 nm over the initial 0-50 residue range, followed by a stable average of 0.05 nm from residues 50 to 197, reflecting a shift toward sustained structural rigidity. Likewise, the 5FU-3QKD complex exhibits a reduction in RMSF from 0.12 nm to 0.05 nm within the 0-50 residue segment, maintaining a stable average of 0.05 nm from residues 50 to 197, indicating a similar stabilization pattern with negligible difference. This similarity suggests that both complexes undergo comparable conformational adjustments, with minimal variation in flexibility. Thus, the magnolialide-3QKD and 5FU-3QKD complexes attain enhanced structural uniformity and reduced flexibility beyond residue 50, underscoring their capacity to maintain stable molecular interactions within the 3QKD protein active site.

The Rg quantifies the compactness of a protein by determining the root mean square distance of all atoms from the protein's center of mass, thereby providing insight into its spatial arrangement [35]. A reduced Rg value signifies a more condensed conformation, whereas an elevated Rg value denotes a more extended structure. The evaluation of Rg values for the complexes is presented in Fig. 5C. The Rg values for the magnolialide-3QKD and 5FU-3QKD complexes exhibited consistent variations between 1.4 and 1.45 nm, with an average of approximately 1.425 nm over the 100 ns simulation period, indicating that both complexes maintain a uniformly compact organization of the 3QKD protein throughout the simulation duration.

Hydrogen bonds play a critical role in molecular dynamics simulations, significantly affecting structural stability, conformational dynamics, and intermolecular interactions [36]. The occurrence of hydrogen bonds remained consistent throughout the 100 ns simulation period, with the magnolialide-3QKD complex displaying a range of 1 to 4 bonds, and the 5FU-3QKD complex exhibiting 1 to 3 bonds. These results indicate that both complexes sustain a stable interaction within the 3QKD protein binding site over the simulation duration, with the magnolialide-3QKD complex showing a slightly higher maximum number of hydrogen bonds compared to the 5FU-3QKD complex (Fig. 5D). This difference suggests that magnolialide establishes a marginally more extensive hydrogen bonding network with the 3QKD protein.

The SASA holds significance in elucidating molecular interactions, especially in biological contexts, as it pertains to protein folding, ligand binding, and overall molecular dynamics [37]. The SASA values underwent assessment to examine the solvent exposure properties of the magnolialide-3QKD and 5FU-3QKD complexes. Examination of the SASA profile revealed dynamic changes over the 100 ns simulation period, with both complexes displaying variations between 75 and 87 nm^2, resulting in an average value of approximately 80 nm^2 (Fig. 5E). These variations indicate ligand-induced modifications in solvent accessibility, reflecting adjustments at the 3QKD-ligand interface that may affect binding properties. The uniformity in fluctuation range and comparable average values across both complexes suggests a stable preservation of the solvent-exposed surface, despite the more favorable docking binding energy of magnolialide (-7.65 kcal mol^{-1}) compared to 5FU (-3.58 kcal mol^{-1}), implying potential differences in binding mechanisms.

The comprehensive evaluation of dynamic parameters has yielded a detailed understanding of the stability and structural properties of the magnolialide-3QKD and 5FU-3QKD complexes, highlighting the 3QKD protein's role in molecular interactions. The analysis demonstrated that the magnolialide-3QKD complex displays greater stability compared to the 5FU-3QKD complex's association with the 3QKD protein, positioning magnolialide as a promising candidate. These findings, consistent with the more favorable docking binding energy of magnolialide (-7.65 kcal mol^{-1}) relative to 5FU (-3.58 kcal mol^{-1}), emphasize its ability to sustain strong binding with the 3QKD protein.

Drug Likeness and ADMET Prediction

ADMET assessments were conducted using the pkCSM platform to examine the oral bioavailability of magnolialide and 5FU, with detailed results presented in Table 2. ADMET assessments were conducted using the pkCSM platform to examine the oral bioavailability of magnolialide and 5FU, with detailed results presented in Table 2. Magnolialide exhibited a human intestinal absorption of 96.886%, exceeding the 91.698% observed for 5FU.

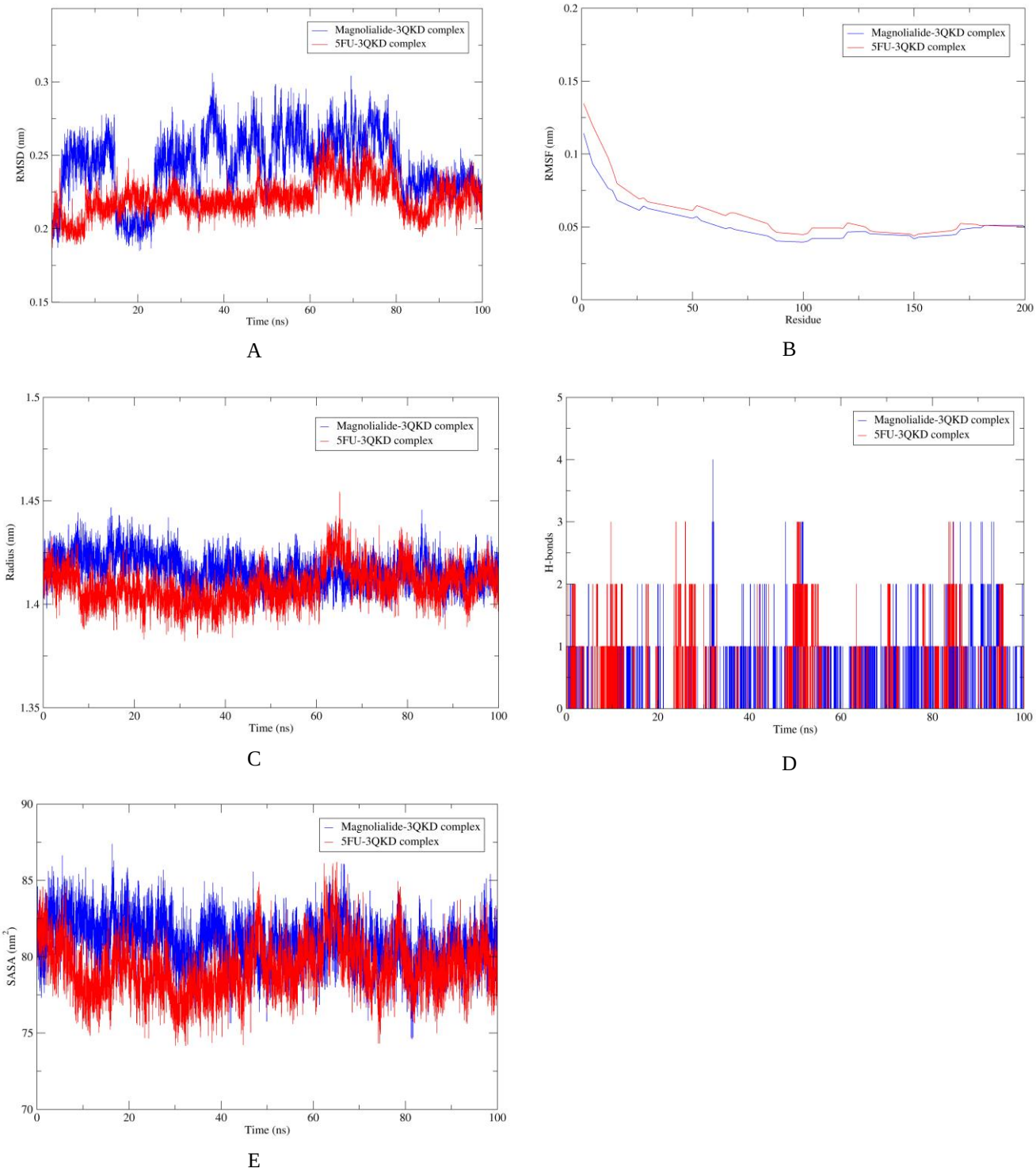

Fig. 5. Results of MD simulation of magnolialide (blue) and 5FU (red) with 3QKD protein. (A) RMSD, (B) RMSF, (C) Rg, (D) H-bonds, (E) SASA.

Both compounds surpass minimal absorption thresholds, ensuring adequate gastrointestinal bioavailability, with magnolialide showing a slight advantage. Water solubility favored 5FU at -1.555 log M relative to -3.032 log M for magnolialide. Caco2 permeability was higher for magnolialide (1.31 log Papp in 10^{-6} cm s^{-1}) compared to 0.559 log Papp in 10^{-6} cm s^{-1} for 5FU, indicating superior membrane permeability. Neither magnolialide nor 5FU acts as a P-glycoprotein substrate or inhibitor (I or II), potentially enhancing bioavailability by avoiding efflux mechanisms, though the lower permeability of 5FU may restrict its absorption efficiency *in vivo*.

Distribution characteristics for magnolialide indicated a limited volume of distribution (VDss 0.209 log l kg^{-1}), differing from the broader distribution observed for 5FU at -0.23 log l kg^{-1}. Blood-brain barrier (BBB) permeability thresholds classify log BB values >0.3 as favorable and <-1 as unfavorable. Magnolialide's log BB of 0.087 suggests moderate permeability, whereas the log BB of 5FU at -0.388 indicates reduced traversal. Central nervous system (CNS) permeability standards designate log PS values >-2 as permeable and <-3 as impermeable. Magnolialide at -2.82 displays limited CNS penetration, while 5FU at -3.039 exhibits even lower access. Fraction unbound (Fu) values recorded magnolialide at 0.409 compared to 0.756 for 5FU, reflecting a higher free fraction for magnolialide to enhance distribution, whereas the elevated Fu of 5FU implies reduced protein binding and potential bioavailability constraints.

Table 2. Predicted ADMET Properties of Magnolialide and 5FU

ADMET properties	Unit	Magnolialide	5FU
Water Solubility	(log M)	-3.032	-1.555
Caco2 permeability	(log Papp in 10-6 cm s^{-1})	1.31	0.559
Intestinal absorption (Human)	(% Absorbed)	96.886	91.698
Skin permeability	(log Kp)	-3.246	-3.725
P-glycoprotein substrate	Yes/No	No	No
P-glycoprotein I inhibitor	Yes/No	No	No
P-glycoprotein II inhibitor	Yes/No	No	No
VDss	(log l kg^{-1})	0.209	-0.23
Fraction unbound (human)	(Fu)	0.409	0.756
BBB permeability	(log BB)	0.087	-0.388
CNS permeability	(log PS)	-2.82	-3.039
CYP2D6 substrate	Yes/No	No	No
CYP3A4 substrate	Yes/No	No	No
CYP1A2 inhibitor	Yes/No	Yes	No
CYP2C19 inhibitor	Yes/No	No	No
CYP2C9 inhibitor	Yes/No	No	No
CYP2D6 inhibitor	Yes/No	No	No
CYP3A4 inhibitor	Yes/No	No	No
Total clearance	(log ml/min/kg)	1.136	0.639
Renal OCT2 substrate	Yes/No	No	No
AMES toxicity	Yes/No	No	No
Max. tolerated dose (human)	(log mg/kg/day)	0.409	1.359
hERG I inhibitor	Yes/No	No	No
hERG II inhibitor	Yes/No	No	No
Oral rat acute toxicity (LD50)	(mol kg^{-1})	2.103	1.939
Oral rat chronic toxicity (LOAEL)	(log mg/kg_bw/day)	1.698	1.587
Hepatotoxicity	Yes/No	No	No
Skin sensation	Yes/No	No	No
T. Pyriformis toxicity	(log ug l^{-1})	0.6	-0.236
Minnow toxicity	(log mM)	1.46	3.152

Metabolic profiles for magnolialide and 5FU underwent evaluation using the pkCSM platform. Neither magnolialide nor 5FU serves as a substrate for CYP2D6 or CYP3A4, indicating no significant metabolism via these cytochrome P450 enzymes. Magnolialide demonstrates inhibitory activity against CYP1A2, while 5FU shows no inhibition across all tested cytochrome P450 isoforms, including CYP1A2, CYP2C19, CYP2C9, CYP2D6, and CYP3A4. The absence of inhibitory effects from 5FU across these isoforms suggests a lower potential for drug-drug interactions mediated by cytochrome P450 metabolism. In contrast, the inhibitory action of magnolialide on CYP1A2 may influence the metabolism of co-administered compounds, potentially affecting therapeutic outcomes.

Excretion characteristics underwent assessment to define clearance profiles of magnolialide and 5FU as potential therapeutic agents prior to elimination. Predicted total clearance for magnolialide reached 1.136 log ml/min/kg, surpassing the 0.639 log ml/min/kg observed for 5FU, indicating a more rapid systemic clearance for magnolialide. This difference, alongside the absence of renal OCT2 substrate activity in both compounds, suggests prolonged retention for 5FU, potentially allowing less frequent dosing. The higher clearance rate of magnolialide may require more frequent administration to maintain therapeutic levels, yet its binding energy of -7.65 kcal mol^{-1} ensures strong target interaction despite accelerated clearance.

Toxicity profiles underwent evaluation to determine the safety characteristics of magnolialide and 5-fluorouracil (5FU). Neither magnolialide nor 5FU exhibited AMES toxicity, indicating no mutagenic potential. The maximum tolerated dose for magnolialide reached 0.409 log mg/kg/day, lower than 1.359 log mg/kg/day for 5FU. Both compounds showed no hERG I or hERG II inhibition, reducing cardiac risk. Oral rat acute toxicity (LD50) values were 2.103 mol kg^{-1} for magnolialide and 1.939 mol kg^{-1} for 5FU, with chronic toxicity (LOAEL) at 1.698 log mg/kg_bw/day and 1.587 log mg/kg_bw/day, respectively. Absence of hepatotoxicity and skin sensation supports safety. Magnolialide's binding energy of -7.65 kcal mol^{-1} with 3QKD enhances anticancer potential for colorectal cancer cells, requiring further *in vivo* validation.

From the in silico ADMET assessments of magnolialide and 5FU, magnolialide presents a favorable pharmacokinetic profile, marked by enhanced absorption, moderate distribution, inactive metabolism, and regulated clearance, despite a lower maximum tolerated dose. Its strong binding to 3QKD (-7.65 kcal mol^{-1}) highlights potential as a candidate for anticancer therapy, targeting colorectal cancer cells through apoptosis modulation. Magnolialide may serve as a foundation for developing derivatives with improved safety, increased effectiveness, and innovative apoptosis-regulating pathways.

Free Binding Energy (MMGBSA) Analysis

Binding free energies of the complexes underwent calculation using the MM/GBSA method in gmx_MMPBSA with the charmm36-jul2022.ff force field. Binding energy (ΔG_binding) derives from G_complex - (G_receptor + G_ligand), or ΔH - TΔS, where effective free energy estimates without entropy are used for comparative affinity assessments. Effective binding energy averaged from 125 snapshots at 80 ps intervals (20-100 ns) captured dynamic protein-ligand interactions under simulated conditions. MMGBSA values appear in Table 3. Effective free energies recorded -17.47 kcal mol^{-1} for magnolialide-3QKD and -1.89 kcal mol^{-1} for 5FU-3QKD, indicating greater affinity for magnolialide, consistent with docking results favoring magnolialide over 5FU.

Quantum Chemistry Computation Using the DFT Method

Density Functional Theory (DFT) is a powerful computational method in quantum chemistry used to determine the electronic structure of atoms, molecules, and materials. It focuses on analyzing the electron density distribution to understand molecular properties. DFT is a widely used tool due to its balance of accuracy and computational efficiency compared to other quantum mechanical methods [38]. Magnolialide and 5FU underwent DFT studies to examine reactivity with the target protein, yielding distinct results as presented in Table 4. The HOMO and LUMO surfaces provided key understanding of structural characteristics, reactivity, and binding patterns for these molecules, as shown in Fig. 6. These orbitals hold importance in electron-transfer processes between molecules and targets. HOMO energy reflects the capacity for electron donation, while LUMO energy indicates potential for electron

Table 3. Free Energy of Binding Obtained Using MMGBSA (kcal mol^{-1})

N°	Magnolialide-3QKD	5FU-3QKD	N°	Magnolialide-3QKD	5FU-3QKD
ΔBOND	-0.00	0.00	Δ1-4 VDW	-0.00	-0.00
ΔANGLE	0.00	-0.00	Δ1-4 E_{EL}	-0.00	-0.00
ΔDIHED	-0.00	0.00	ΔE_{GB}	15.93	4.88
ΔUB	0.00	0.00	ΔE_{SURF}	-3.04	-0.48
ΔIMP	-0.00	0.00	ΔG_{GAS}	-30.36	-6.29
ΔCMAP	0.00	0.00	ΔG_{SOLV}	12.88	4.40
ΔVDWAALS	-22.92	-3.00	**ΔTOTAL**	**-17.47**	**-1.89**
ΔE_{EL}	-7.44	-3.29			

Table 4. Quantum Desciptors of Magnolialide and 5FU

Molecule	EHOMO (eV)	ELUMO (eV)	ΔE (eV)	μ (eV)	χ (eV)	η (eV)	σ (eV^{-1})	ω (eV)
Magnolialide	-9.0271	2.6025	11.6296	-3.2123	3.2123	5.8148	0.1720	0.8873
5FU	-10.1458	2.3631	12.5089	-3.8914	3.8914	6.2545	0.1599	1.2105

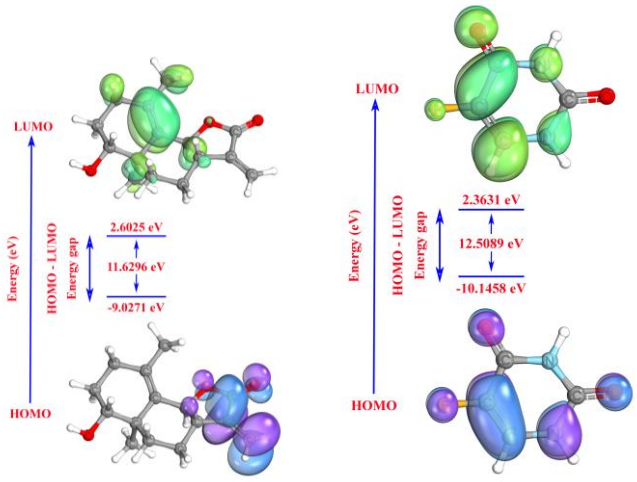

A B

Fig. 6. HOMO and LUMO surface diagrams of magnolialide (A), and 5FU (B).

acceptance. Magnolialide exhibits a higher EHOMO (−9.0271 eV) than 5FU (−10.1458 eV), suggesting greater susceptibility to oxidation and enhanced electron-donation ability. The lowest LUMO energy appears in 5FU (−2.3631 eV), implying superior electron-acceptance compared to magnolialide (−2.6025 eV). The energy gap ΔE serves as an indicator of stability and reactivity, with smaller values denoting elevated reactivity and reduced stability, whereas larger gaps signify increased stability [38,39]. 5FU displays the largest ΔE (12.5089 eV), indicating superior stability and lower reactivity among the compounds. Magnolialide possesses the smallest gap (11.6296 eV), potentially rendering it more reactive and bioactive. Ionization potential (IP) quantifies the energy required for electron removal, where a higher IP implies greater resistance to oxidation. Electron affinity (EA) evaluates electron-acceptance capability, with elevated values signifying stronger affinity and electron-acceptor behavior [40]. Magnolialide shows lower IP compared to 5FU, denoting easier electron loss. 5FU exhibits higher EA, suggesting greater readiness to accept electrons and amplified electrophilic traits. Chemical hardness (η) relates to resistance against electron cloud distortion, while softness (σ) represents the reciprocal of hardness and indicates reactivity ease [41,42]. 5FU presents the highest hardness (6.2545 eV), reflecting robust resistance to electronic changes, consistent with elevated stability. Magnolialide demonstrates lower hardness (5.8148 eV) and higher softness (0.1720 eV^{-1}) than 5FU (0.1599 eV^{-1}), implying greater reactivity and

bioactivity prospects. Electronegativity (χ) measures attraction toward electron density. Values demonstrate moderate to elevated electronegativity across compounds, with 5FU registering the highest (3.8914 eV). Chemical potential (μ) denotes propensity for electron exchange, where negative values suggest electron-gain tendency [43]. 5FU features a lower value (−3.8914 eV), indicating stronger electron-acceptance. The electrophilicity index (ω) assesses electrophilic strength. Higher ω values reflect pronounced electrophilic behavior [44,45]. 5FU holds the highest electrophilicity (1.2105 eV), signifying robust electron-attraction and interaction potential with biological targets.

CONCLUSIONS

The investigation incorporated molecular docking, dynamics simulations, ADMET predictions, and DFT calculations to assess magnolialide, focusing on interaction with Bcl-xL (protein ID: 3QKD). Docking findings demonstrated enhanced binding affinity and alignment of magnolialide at the 3QKD site compared to 5FU. Dynamics simulations spanning 100 ns verified stable association in the magnolialide-3QKD complex, affirming reliable engagement with this anti-apoptotic regulator. DFT examination disclosed unique reactivity patterns, wherein magnolialide exhibited elevated HOMO energy and reduced LUMO energy compared to 5FU, with a smaller energy gap, implying amplified reactivity and electron-donation capacity, alongside diminished hardness and augmented softness. These results endorse magnolialide as a prospective modulator of Bcl-xL to induce apoptosis in colorectal cancer cells. Computational data demand experimental substantiation. Future investigations should emphasize *in vitro* and *in vivo* evaluations to rigorously analyze interactions involving magnolialide, including impacts on efficacy and safety within cellular contexts.

REFERENCES

[1] Bray, F.; Laversanne, M.; Sung, H.; Ferlay, J.; Siegel, R. L.; Soerjomataram, I.; Jemal, A., Global cancer statistics 2022: GLOBOCAN estimates of incidence and mortality worldwide for 36 cancers in 185 countries. *CA. Cancer J. Clin.* **2024**, *74* (3), 229-263, DOI: 10.3322/caac.21834.

[2] Fu, M.; Li, Y.; Wang, J., Incidence and Mortality of Colorectal Cancer in Asia in 2022 and Projections for 2050. *J. Gastroenterol. Hepatol.* **2025**, *40* (5), 1143-1156, DOI: 10.1111/jgh.16910.

[3] Xi, Y.; Xu, P., Global colorectal cancer burden in 2020 and projections to 2040. *Transl. Oncol.* **2021**, *14* (10), 101174, DOI: 10.1016/j.tranon.2021.101174.

[4] Yeo, M. R.; Voutsadakis, I. A., Characteristics, Treatment and Outcomes of Stage I to III Colorectal Cancer in Patients Aged over 80 Years Old. *Cancers* **2025**, *17* (2), 247, DOI: 10.3390/cancers17020247.

[5] Morales, C. S.; Grodzinski, P., Current landscape of treating different cancers using nanomedicines: Trends and perspectives. *Wiley Interdiscip. Rev. Nanomed. Nanobiotechnol.* **2024**, *16* (1), e1927, 10.1002/wnan.1927.

[6] Davison, E. K.; Brimble, M. A., Natural product derived privileged scaffolds in drug discovery. *Curr. Opin. Chem. Biol.* **2019**, *52*, 1-8, DOI: 10.1016/j.cbpa.2018.12.007.

[7] Zeng, T.; Li, J.; Wu, R., Natural product databases for drug discovery: Features and applications. *Pharm. Sci. Adv.* **2024**, *2*, 100050, DOI: 10.1016/j.pscia.2024.100050.

[8] Xu, S.; Tang, Y.; Li, Y.; Yang, J.; Gu, W.; Hao, X.; Yuan, C., Discovery of diverse sesquiterpenoids from *Magnolia grandiflora* with cytotoxic activities by inducing cell apoptosis. *Bioorg. Chem.* **2023**, *139*, 106707, DOI: 10.1016/j.bioorg.2023.106707.

[9] Jiao, X.; Jin, X.; Ma, Y.; Yang, Y.; Li, J.; Liang, L.; Liu, R.; Li, Z., A comprehensive application: Molecular docking and network pharmacology for the prediction of bioactive constituents and elucidation of mechanisms of action in component-based Chinese medicine. *Comput. Biol. Chem.* **2021**, *90*, 107402, DOI: 10.1016/j.compbiolchem.2020.107402.

[10] Zhang, G.; Li, Q.; Chen, Q.; Su, S., Network Pharmacology: A New Approach for Chinese Herbal Medicine Research. *Evidence-Based Complement. Altern. Med.* **2013**, *2013* (1), 621423, DOI: 10.1155/2013/621423.

[11] Noor, F.; Tahir ul Qamar, M.; Ashfaq, U. A.; Albutti, A.; Alwashmi, A. S. S.; Aljasir, M. A., Network Pharmacology Approach for Medicinal Plants: Review and Assessment. *Pharmaceuticals* **2022**, *15* (5), 572, DOI: 10.3390/ph15050572.

[12] Sleebs, B. E.; Czabotar, P. E.; Fairbrother, W. J.; Fairlie, W. D.; Flygare, J. A.; Huang, D. C. S.; Kersten, W. J. A.; Koehler, M. F. T.; Lessene, G.; Lowes, K.; Parisot, J. P.; Smith, B. J.; Smith, M. L.; Souers, A. J.; Street, I. P.; Yang, H.; Baell, J. B., Quinazoline Sulfonamides as Dual Binders of the Proteins B-Cell Lymphoma 2 and B-Cell Lymphoma Extra Long with Potent Proapoptotic Cell-Based Activity. *J. Med. Chem.* **2011**, *54* (6), 1914-1926, DOI: 10.1021/jm101596e.

[13] Laskowski, R. A.; MacArthur, M. W.; Moss, D. S.; Thornton, J. M., PROCHECK: a program to check the stereochemical quality of protein structures. *J. Appl. Crystallogr.* **1993**, *26* (2), 283-291, DOI: 10.1107/S0021889892009944.

[14] Van Der Spoel, D.; Lindahl, E.; Hess, B.; Groenhof, G.; Mark, A. E.; Berendsen, H. J. C., GROMACS: Fast, flexible, and free. *J. Comput. Chem.* **2005**, *26* (16), 1701-1718, DOI: 10.1002/jcc.20291.

[15] Guex, N.; Peitsch, M. C., SWISS-MODEL and the Swiss-Pdb Viewer: An environment for comparative protein modeling. *Electrophoresis* **1997**, *18* (15), 2714-2723, DOI: 10.1002/elps.1150181505.

[16] Zoete, V.; Cuendet, M. A.; Grosdidier, A.; Michielin, O., SwissParam: A fast force field generation tool for small organic molecules. *J. Comput. Chem.* **2011**, *32* (11), 2359-2368, DOI: 10.1002/jcc.21816.

[17] Pettersen, E. F.; Goddard, T. D.; Huang, C. C.; Couch, G. S.; Greenblatt, D. M.; Meng, E. C.; Ferrin, T. E., UCSF Chimera - A visualization system for exploratory research and analysis. *J. Comput. Chem.* **2004**, *25* (13), 1605-1612, DOI: 10.1002/jcc.20084.

[18] Tao, L.; Zhang, P.; Qin, C.; Chen, S. Y.; Zhang, C.; Chen, Z.; Zhu, F.; Yang, S. Y.; Wei, Y. Q.; Chen, Y. Z., Recent progresses in the exploration of machine learning methods as in-silico ADME prediction tools. *Adv. Drug Deliv. Rev.* **2015**, *86*, 83-100, DOI: 10.1016/j.addr.2015.03.014.

[19] Pires, D. E. V; Blundell, T. L.; Ascher, D. B., pkCSM: Predicting Small-Molecule Pharmacokinetic and Toxicity Properties Using Graph-Based Signatures. *J. Med. Chem.* **2015**, *58* (9), 4066-4072, DOI: 10.1021/acs.jmedchem.5b00104.

[20] Genheden, S.; Ryde, U., The MM/PBSA and MM/GBSA methods to estimate ligand-binding affinities. *Expert Opin. Drug Discov.* **2015**, *10* (5), 449-461, DOI: 10.1517/17460441.2015.1032936.

[21] Nyangiwe, N. N., Applications of density functional theory and machine learning in nanomaterials: A review. *Next Mater.* **2025**, *8*, 100683, DOI: 10.1016/j.nxmate.2025.100683.

[22] Neese, F., Software Update: The ORCA Program System-Version 6.0. *WIREs Comput. Mol. Sci.* **2025**, *15* (2), e70019, DOI: 10.1002/wcms.70019.

[23] Knizia, G.; Klein, J. E., Electron Flow in Reaction Mechanisms-Revealed from First Principles. *Angew. Chemie Int. Ed.* **2015**, *54* (18), 5518-5522, DOI: 10.1002/anie.201410637.

[24] Knizia, G., Intrinsic Atomic Orbitals: An Unbiased Bridge between Quantum Theory and Chemical Concepts. *J. Chem. Theory Comput.* **2013**, *9* (11), 4834-4843, DOI: 10.1021/ct400687b.

[25] Hanwell, M. D.; Curtis, D. E.; Lonie, D. C.; Vandermeersch, T.; Zurek, E.; Hutchison, G. R., Avogadro: an advanced semantic chemical editor, visualization, and analysis platform. *J. Cheminform.* **2012**, *4* (1), 17, DOI: 10.1186/1758-2946-4-17.

[26] Luo, J.; Xue, Z. Q.; Liu, W. M.; Wu, J. L.; Yang, Z. Q., Koopmans' Theorem for Large Molecular Systems within Density Functional Theory. *J. Phys. Chem. A* **2006**, *110* (43), 12005-12009, DOI: 10.1021/jp063669m.

[27] Das, R.; Vigneresse, J. -L.; Chattaraj, P. K., Chemical reactivity through structure-stability landscape. *Int. J. Quantum Chem.* **2014**, *114* (21), 1421-1429, DOI: 10.1002/qua.24706.

[28] Agu, P. C.; Afiukwa, C. A.; Orji, O. U.; Ezeh, E. M.; Ofoke, I. H.; Ogbu, C. O.; Ugwuja, E. I.; Aja, P. M., Molecular docking as a tool for the discovery of molecular targets of nutraceuticals in diseases management. *Sci. Rep.* **2023**, *13* (1), 13398, DOI: 10.1038/s41598-023-40160-2.

[29] Shamsian, S.; Sokouti, B.; Dastmalchi, S., Benchmarking different docking protocols for predicting

the binding poses of ligands complexed with cyclooxygenase enzymes and screening chemical libraries. *Bioimpacts* **2024**, *14* (2), 29955, DOI: 10.34172/bi.2023.29955.

[30] Patil, R.; Das, S.; Stanley, A.; Yadav, L.; Sudhakar, A.; Varma, A. K., Optimized Hydrophobic Interactions and Hydrogen Bonding at the Target-Ligand Interface Leads the Pathways of Drug-Designing. *PLoS One* **2010**, *5* (8), e12029, DOI: 10.1371/journal.pone.0012029 .

[31] Barratt, E.; Bingham, R. J.; Warner, D. J.; Laughton, C. A.; Phillips, S. E. V; Homans, S. W., Van der Waals Interactions Dominate Ligand-Protein Association in a Protein Binding Site Occluded from Solvent Water. *J. Am. Chem. Soc.* **2005**, *127* (33), 11827-11834, DOI: 10.1021/ja0527525.

[32] Stollar, E. J.; Smith, D. P., Uncovering protein structure. *Essays Biochem.* **2020**, *64* (4), 649-680, DOI: 10.1042/EBC20190042.

[33] Hassan, A. M.; Gattan, H. S.; Faizo, A. A.; Alruhaili, M. H.; Alharbi, A. S.; Bajrai, L. H.; AL-Zahrani, I. A.; Dwivedi, V. D.; Azhar, E. I., Evaluating the Binding Potential and Stability of Drug-like Compounds with the Monkeypox Virus VP39 Protein Using Molecular Dynamics Simulations and Free Energy Analysis. *Pharmaceuticals* **2024**, *17* (12), 1617, DOI: 10.3390/ph17121617.

[34] Kumar, M.; Tripathi, M. K.; Kaur, P., *Structure-Based Drug Design*. Cham: Springer International Publishing, **2024**, pp. 149-175.

[35] Bagewadi, Z. K.; Yunus Khan, T. M.; Gangadharappa, B.; Kamalapurkar, A.; Mohamed Shamsudeen, S.; Yaraguppi, D. A., Molecular dynamics and simulation analysis against superoxide dismutase (SOD) target of *Micrococcus luteus* with secondary metabolites from *Bacillus licheniformis* recognized by genome mining approach. *Saudi J. Biol. Sci.* **2023**, *30* (9), 103753, DOI: 10.1016/j.sjbs.2023.103753.

[36] Zheng, Y.; Shen, R.; Dai, Y.; Xie, Y.; Wang, C.; Cai, Y.; Wang, K., Hydrogen Bonds Mediating the Structural and Dynamic Behaviors in Choline-Phenolic Acid Ionic Liquids: A Computational Investigation. *J. Phys. Chem. B* **2025**, *129* (25), 6265-6275, DOI: 10.1021/acs.jpcb.5c01232.

[37] Mahmoud, A. H.; Masters, M. R.; Yang, Y.; Lill, M. A., Elucidating the multiple roles of hydration for accurate protein-ligand binding prediction via deep learning. *Commun. Chem.* **2020**, *3* (1), 19, DOI: 10.1038/s42004-020-0261-x.

[38] Van Mourik, T.; Bühl, M.; Gaigeot, M. P., Density functional theory across chemistry, physics and biology. *Philos. Trans. R. Soc. A Math. Phys. Eng. Sci.* **2014**, *372* (2011), 20120488, DOI: 10.1098/rsta.2012.0488.

[39] Azeez, Y. H.; Kareem, R. O.; Qader, A. F.; Omer, R. A.; Ahmed, L. O., Spectroscopic characteristics, stability, reactivity, and corrosion inhibition of AHPE-dop compounds incorporating (B, Fe, Ga, Ti): A DFT investigation. *Next Mater.* **2024**, *3*, 100184, DOI: 10.1016/j.nxmate.2024.100184.

[40] Oono, T.; Okada, T.; Sasaki, T.; Inagaki, K.; Ushiku, T.; Shimizu, T.; Hatakeyama, T.; Fukagawa, H., Unlocking the Full Potential of Electron-Acceptor Molecules for Efficient and Stable Hole Injection. *Adv. Mater.* **2023**, *35* (11), 2210413, DOI: 10.1002/adma.202210413.

[41] Gázquez, J. L., *Chemical Hardness*. Berlin: Springer, **1993**, pp. 27-43.

[42] Talmaciu, M. M.; Bodoki, E.; Oprean, R., Global chemical reactivity parameters for several chiral beta-blockers from the Density Functional Theory viewpoint. *Clujul Med.* **2016**, *89* (4), 513, DOI: 10.15386/cjmed-610.

[43] Zerón, P.; Pantoja-Hernández, M. A.; Franco-Pérez, M.; Gázquez, J. L., Local and non-local chemical potential and hardness: a grand canonical ensemble approach. *J. Mol. Model.* **2025**, *31* (3), 90, DOI: 10.1007/s00894-025-06311-0.

[44] Parthasarathi, R.; Subramanian, V.; Roy, D. R.; Chattaraj, P. K., Electrophilicity index as a possible descriptor of biological activity. *Bioorg. Med. Chem.* **2004**, *12* (21), 5533–5543, DOI: https://doi.org/10.1016/j.bmc.2004.08.013.

[45] Domingo, L. R.; Aurell, M. J.; Pérez, P.; Contreras, R., Quantitative characterization of the global electrophilicity power of common diene/dienophile pairs in Diels-Alder reactions. *Tetrahedron* **2002**, *58* (22), 4417-4423, DOI: 10.1016/S0040-4020(02)00410-6.